Modeling Excess Retrieval in Rat Melanotroph Membrane Capacitance Records

Igor Poberaj,[†] Marjan Rupnik,[*] Marko Kreft,[*§] Sujit K. Sikdar,[*‡] and Robert Zorec[*]

[*]Laboratory of Neuroendocrinology–Molecular Cell Physiology, Institute of Pathophysiology, Medical School, and [†]Department of Physics, Faculty of Mathematics and Physics, 1001 Ljubljana, Slovenia; [‡]Molecular Biophysics Unit, Indian Institute of Science, Bangalore 560012, India; and [§]Celica, Biomedical Sciences Center, 1000 Ljubljana, Slovenia

ABSTRACT We have used the patch-clamp technique to monitor changes in membrane capacitance (C_m) elicited by fast and spatially homogeneous rises in cytosolic calcium concentration ($[Ca^{2+}]_i$) using flash photolysis of NP-EGTA. Average peak $[Ca^{2+}]_i$ amplitudes of 20–25 μM triggered three different types of responses in C_m: (i) In 42% of cells, a rise in $[Ca^{2+}]_i$ activated a monotonic increase in C_m followed by a slow decline to resting values; (ii) In 30% of cells, the rise in C_m was clearly characterized by two dynamic components, consisting of a rapid and a slow exo–endocytosis cycle; (iii) In 28% of cells, after the initial rapid rise in C_m, endocytosis exhibited excess retrieval that was characterized by a decline in C_m below resting C_m. The aim of this work is to develop a unified mathematical model with a minimum number of parameters that would describe all the observed types of responses. Three models were considered: Model A, a model with a single component of exo-endocytosis cycle; model B, a model consisting of a sum of two independent dynamic components; and model C, a model in which, in addition to the two dynamic components as in model B, excess retrieval due to a lipid flow through the reversal closing of the fusion pore during the rapid component of exo-endocytosis cycle was considered. The results show that the latter model describes all the types of responses in C_m recorded in rat melanotrophs. The association of excess retrieval exclusively with the rapid, but not the slow, exocytosis indicates that some fusing vesicles mediate a lipidic flux during the reversal closing of the fusion pore, whereas those entering the slow phase of exocytosis may fuse with the plasma membrane completely and are retrieved by other endocytic machinery, independent of the lipid flow that might have occurred as the fusion pore opened permanently.

INTRODUCTION

The application of caged-Ca^{2+} compounds to study Ca^{2+}-dependent exocytosis by membrane capacitance (C_m) measurements has revealed multiple kinetic components (Kasai, 1999). There are two views about the nature of this kinetic diversity. First, a sequence of intermediates of a homogeneous population of vesicles may result in multiple kinetic components (Heinemann et al., 1994, Thomas et al., 1993, Xu et al., 1998). Second, heterogeneous populations of vesicles engaged in distinct pathways of exocytosis may also result in multiple kinetic components (Voets, 2000). Although the quantitative C_m measurements cannot readily distinguish the contributions of heterogeneous vesicles or vesicle intermediates, a combination with other approaches was used to address this problem. Using serotonin-loaded dense-core vesicles and amperometry, it was shown that, in pancreatic β-cells, two populations of dense-core granules enter distinct pathways of exocytosis (Takahashi et al., 1997). Using myoballs to monitor the release of acetylcholine from PC12 cells, it was demonstrated that exocytosis of synaptic vesicles and dense-core granules consists of distinct pathways (Ninomiya et al., 1997). By using an antibody to Ca^{2+}-dependent activator protein for secretion (CAPS), a neural/endocrine-specific 145-kD protein, originally characterized as a brain cytosolic factor that reconstitutes Ca^{2+}-dependent secretion in permeable neuroendocrine cells (Walent et al., 1992), it was shown that the rapid component of secretory response in rat melanotrophs was selectively abolished (Rupnik et al., 2000), whereas an antibody selective for the heterotrimeric $G\alpha_{i3}$ attenuated the slow phase of exocytosis (Kreft et al. 1999), suggesting that the two kinetically and biochemically distinct phases of C_m increase represent distinct exocytotic pathways in melanotrophs. To understand the nature of this highly complex process, a suitable model of membrane turnover dynamics would be of great benefit. Therefore, the aim of this work is to establish a model describing flash-induced time-dependent changes in C_m.

Using rat melanotrophs, which secrete pro-opiomelanocortin-derived peptides via dense-core vesicle exocytosis (Mains and Eipper, 1979), we have used C_m measurements (Neher and Marty, 1982) combined with flash photolysis to deliver rapid and spatially homogeneous steps in cytosolic Ca^{2+} (Neher and Zucker, 1993), which elicit multiple kinetic components in secretory activity. As reported previously (Thomas et al., 1993, 1994; Rupnik et al., 2000), we confirmed that multiple kinetic components characterized these responses in melanotrophs. It was shown previously that distinct kinetic components display distinct biochemical mechanisms (Kreft et al., 1999; Rupnik et al., 2000), therefore we modeled the time course in C_m to be due to one or a sum

Received for publication 23 October 2000 and in final form 1 October 2001.

Address reprint requests to Robert Zorec, PAFI, Institute of Pathophysiology, Medical School, Laboratory of Neuro-Endocrinology–Molecular Cell Physiology, P.O.B. 2211, 1001 Ljubljana, Slovenia. Tel.: +386-1-543-70-20; Fax: +386-1-543-70-21; E-mail: robert.zorec@mf.uni-lj.si.

0006-3495/02/01/226/07 $2.00

of two independent endo–exocytosis cycles. Furthermore, excess retrieval was observed after the rapid rise in C_m in ~28% of recordings, as reported by Thomas et al. (1994). We model this process by assuming it is due to a lipid flux during reversible fusion-pore opening (Monck et al., 1990). The results show that the model consisting of two dynamic components of exo–endocytosis cycle, with lipid flow taken into account, fits experimental results significantly better than other tested models. Excess retrieval observed after the rapid exocytosis indicates the existence of a functional state of docked vesicles, which mediates a significant lipid flux during the reversal closing of the fusion pore.

MATERIALS AND METHODS

Cell preparation

Melanotrophs were prepared as described by Rupnik and Zorec (1992).

Compensated membrane capacitance measurements

Compensated membrane capacitance measurements were performed as described (Neher and Marty, 1982; Zorec et al. 1991; Rupnik and Zorec; 1995), using a SWAM CELL or SWAM IIB patch-clamp-lock-in amplifier (Celica, Ljubljana, Slovenia), operating at 1.6 kHz. Upon establishment of the whole-cell configuration, C_m and G_a (access conductance) were compensated by C_{slow} and G_a compensation controls. Sine voltage of 11–111 mV_{rms} was applied. The phase angle setting was determined by applying a 100 fF or 1 pF calibration pulse while monitoring the pulse on the *C* (signal proportional to C_m) and *G* outputs of the lock-in amplifier. These two signals were stored unfiltered (C-DAT4, Cygnus Technology, Inc., Delaware Water Gap, PA) for off-line analysis. Simultaneously, we recorded filtered (300 Hz, 4 pole Bessel) *C* and *G* signals, the fluorescence intensity from a C660 photon counter (Thorn EMI, Middlesex, UK) and membrane current (0–10 Hz, low pass Bessel). PhoCal program (LSR, Cambridge, UK) was used to acquire signals every 5 ms. For temporally high resolution measurements of C_m, the data recorded on DAT recorder were played back in 10-s sequences and digitized at 50 kHz using a CDR program (J. Dempster, Strachclyde, UK). Signals were digitally low-pass filtered at 1 kHz (2-way 150th order FIR filter, Math Works MATLAB, Math Works, Natik, MA) and resampled at 10 kHz. The pipette solution contained (in mM): KCl 110, TEACl 10, KOH/HEPES (N-2-hydroxyethylpiperazine-*N*′-2-ethanesulphonic acid) 40, Na_2ATP 2, $MgCl_2$ 2, K_4-NP-EGTA [o-nitrophenyl ethyleneglycol-bis-(β-aminoethyl-ether)-*N*,*N*,*N*′,*N*′-tetrapotassium salt, Molecular Probes, Eugene, OR] 4, $CaCl_2$ 3.6, furaptra 0.5, pH = 7.2. The bath contained (in mM): NaCl 131.8, KCl 5, $MgCl_2$ 2, NaH_2PO_4 0.5, $NaHCO_3$ 5, Na HEPES 10, D-glucose 10, $CaCl_2$ 1.8, pH = 7.2. Recordings were made at room temperature. Pipette resistances ranged from 1 to 4 MΩ.

Flash photolysis and $[Ca^{2+}]_i$ measurements

We used o-nitrophenyl ethyleneglycol-*bis*-(β-aminoethyl-ether)-*N*,*N*,*N*′,*N*′-tetraacetic acid (NP-EGTA) (Molecular Probes) to manipulate $[Ca^{2+}]_i$. A UV flash from a Xe arc flash lamp (Hi-Tech, Salisbury, UK) illuminated cells through a 40× fluor oil immersion objective of a Nikon Diaphot microscope. The same optical pathway was used to illuminate the fluorescent $[Ca^{2+}]$ indicator furaptra (Molecular Probes). Calibration of $[Ca^{2+}]_i$ measurements was performed in each cell (Carter and Ogden, 1994; Kreft et al., 1999) by using the autofluorescence in a cell-attached configuration and the fluorescence in a resting whole-cell recording.

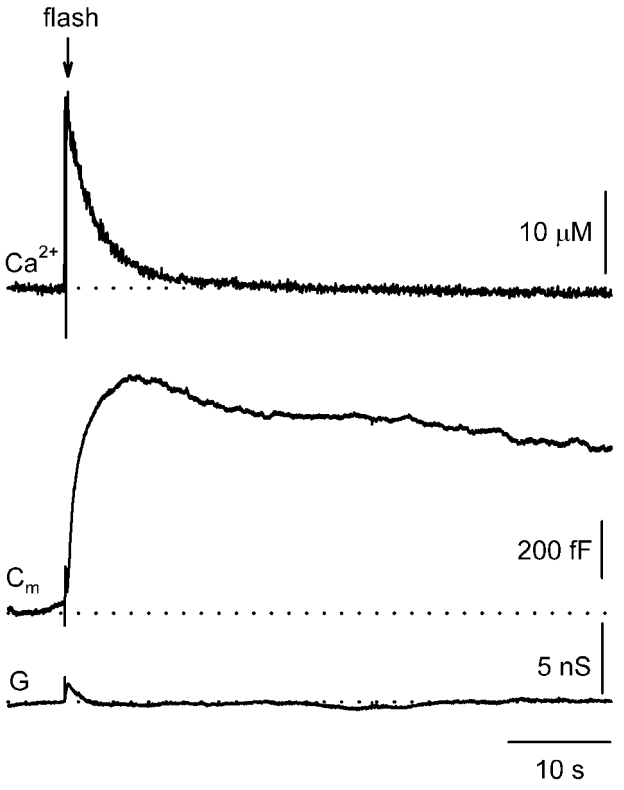

FIGURE 1 Time-dependent changes in $[Ca^{2+}]_i$ (*top trace*), membrane capacitance (C_m), and conductance (*G*, reflecting changes in access conductance, membrane conductance, and C_m) after flash photolysis of Ca^{2+}-loaded NP-EGTA (*arrow*). Dashed lines in the middle and bottom traces indicate resting capacitance of 4.8 pF and access conductance of 150 nS, respectively. Both parameters were determined using the controls on the SWAM patch-clamp amplifier.

Data analysis and modeling

Measured data were analyzed with the Microcal Origin program. First, the time interval of the measurements was truncated to the same length chosen to be five seconds after flash photolysis excitation. Then the data were fitted with functions corresponding to different models. The functions were coded in C and compiled in DLL which was used by the Nonlinear Least Square Fitting (NLSF) procedure built into Origin. Statistics are in the format mean ± SEM.

RESULTS

Classification of flash-induced time-dependent changes in C_m

Resting membrane capacitance (C_m) was stable, averaging 5.3 ± 0.2 pF (mean ± SEM, n = 50), as reported by (Zupančič et al., 1994). Figure 1 shows a typical time course for $[Ca^{2+}]_i$ and C_m during flash photolysis of an NP-EGTA-loaded cell. The arrow on the top indicates the flash (150 V/3.9 mF discharge) delivery to the patched cell through the objective, which photolyzed around 10% of the Ca^{2+}-bound NP-EGTA (see Materials and Methods). This flash tran-

siently increased $[Ca^{2+}]_i$ to 25 μM (Fig. 1, *top trace*), after which $[Ca^{2+}]_i$ dropped back to the baseline with an exponential time constant of ~4 s, due to extrusion from the cell, and due to diffusion into the pipette and mixing with the unphotolyzed cage. After flash delivery, C_m increased by 805 fF and later slowly decreased due to slow endocytosis toward resting C_m of 4.8 pF (Fig. 1, *middle trace*). The prominent increase in C_m was preceded by a smaller (160 fF) transient rise in C_m, termed rapid exocytosis (Rupnik et al., 2000), which is clearly resolved in Fig. 2 *B* at a higher time resolution. The rapid phase is followed by a slower rise in C_m, which was termed slow exocytosis (Rupnik et al., 2000). Conductance trace (Fig. 1, *bottom trace*), reflecting contributions of access conductance, membrane conductance and membrane capacitance (Lindau and Neher, 1988) was not correlated to changes in C_m. When the NP-EGTA filling the cell contained no Ca^{2+} (six cells), the flash did not change $[Ca^{2+}]_i$ and both C_m and conductance remained constant (data not shown).

Membrane capacitance measurements were performed on 54 cells with a transient increase in $[Ca^{2+}]_i$ similar to that seen in Fig. 1 (ranging between 10 and 40 μM). Experiments revealed two other types of changes in C_m during the period of 5 s after the flash delivery (Fig. 2, *A* and *C*). Therefore, the responses in C_m were grouped into three types (Fig. 2). Type A: In 23 cells (42%), C_m responses consisted of a monotonic increase in C_m followed by a decline in C_m similar to that seen in Fig. 1 (*middle trace*). The increase in C_m resembled the slow phase of exocytosis (Rupnik et al., 2000). The presence of an initial rapid component in these responses cannot be excluded, however it was not clearly visible, possibly due to a smaller amplitude representing only 10% of the amplitude of the slow component (see Rupnik et al., 2000). Type B: In 16 cells (30%), C_m rise consisted of a superposition of two clearly visible dynamic components of exo–endocytosis cycle, the rapid and the slow components (Rupnik et al., 2000). Type C: In 15 cells (28%), C_m responses exhibited excess retrieval after the initial rise in C_m. Peak values in $[Ca^{2+}]_i$ eliciting different types of responses were not significantly different: 26.6 ± 0.8 μM (n = 23) for Type A; 23.5 ± 5.6 μM (n = 15) for type B; and 19.9 ± 5.8 μM (n = 16) for Type C response.

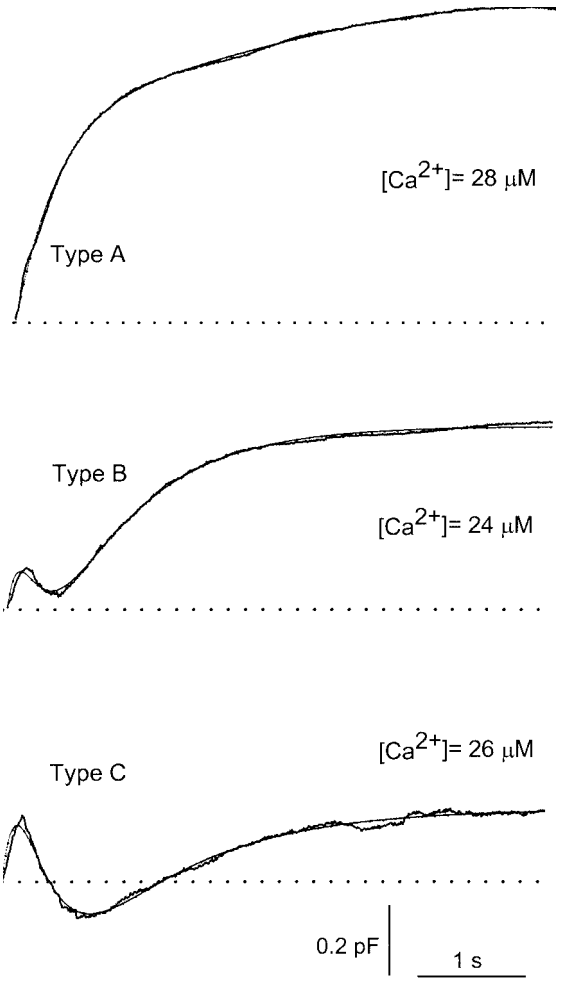

FIGURE 2 Types of responses in flash-induced increases in C_m. *Top*: Type A response is a monotonic increase in C_m, which resembles a single slow phase response. *Middle*: Type B response consists of two dynamically distinct phases in C_m. *Bottom*: Type C response is similar to type B response, but the signal exhibits excess retrieval after the rapid rise in C_m. Curves with dots represent best fits to Eq. 3, where the parameters were as follows: *Top*: B_{0F} = 0.61 pF, B_{0S} = 3.62 pF, α = 1.78, k_F = 1.34 s^{-1}, k_{exoS} = 0.21 s^{-1}, k_{endoS} = 0.2 s^{-1}; *middle*: B_{0F} = 0.14 pF, B_{0S} = 1.04 pF, α = 5.04, k_F = 6.49 s^{-1}, k_{exoS} = 1.27 s^{-1}, k_{endoS} = 0 s^{-1}; *bottom*: B_{0F} = 0.27 pF, B_{0S} = 0.67 pF, α = 2.98, k_F = 4.43 s^{-1}, k_{exoS} = 1.01 s^{-1}, k_{endoS} = 0 s^{-1}.

Fitting different models to the time-courses in C_m

To describe the time course of the three types of responses in C_m (Fig. 2), we consider three models (see Fig. 3 and Appendix). Model A is the simplest and takes only one dynamic component of exo–endocytosis cycle into account (Fig. 3, *top trace*). Note that its applicability is limited only to C_m responses of type A (Fig. 2). To describe responses of type B, Model A is expanded to Model B by adding a second independent dynamic component of exo–endocytic cycle (Fig. 3, *middle trace*). The sum of two independent components implies that the whole process is parallel rather than sequential (Rupnik et al., 2000).

Excess retrieval was observed exclusively in conjunction with the rapid phase of the C_m increase (Fig. 2), consistent with previous reports (Thomas et al., 1994). It has been reported that, during pore opening, a substantial lipid flow between the plasmalemma and the vesicle

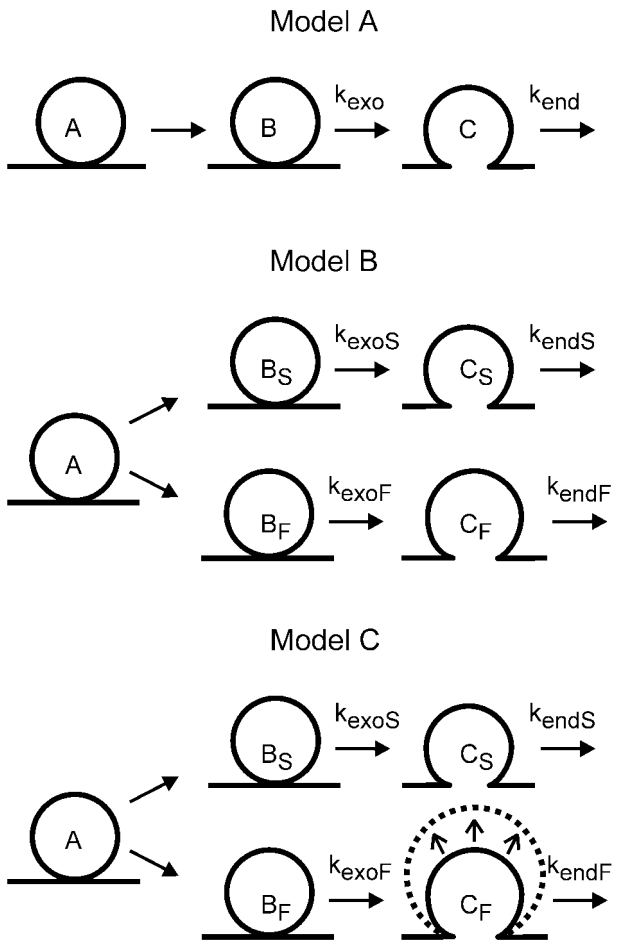

FIGURE 3 Diagram of models of exo–endocytosis cycle in rat melanotrophs. The models are based on the vesicle evolution scheme, where vesicles are grouped into three different pools A, B, and C, according to their evolutionary state. Pool A contains vesicles that have not reached release-ready state yet and thus cannot directly contribute to the measured signal. The contribution of pool A to the capacitance signals in our models can be neglected. Pool B contains vesicles that can be immediately released upon Ca^{2+} stimulation. Released vesicles enter pool C. Measured capacitance is proportional to the number of vesicles in the pool C. Model A (*top*) consists of one exo–endocytosis cycle, k_{exo}, k_{end} represent rate constants. Model B (*middle*) consists of two parallel exo–endocytosis cycles, where subscripts $k_{S,}$ k_F denote slow and fast exo–endocytic pathways, respectively. Model C (*bottom*) is similar to Model B, but a process of excess retrieval was considered to take place in the fast exo–endocytic cycle, depicted by the dashed curve.

membrane can take place, which is driven by a tension gradient between the two membranes (Monck et al., 1990; Chizmadhzev et al., 2000). To describe type C responses in C_m, we refine Model B into Model C by taking the lipid flow associated with the reversal opening of a fusion pore during rapid exocytosis into account (Fig. 3, *bottom*, *dashed line*).

Functional representations of the three models (derived in Appendix) are presented by the Eqs. 1–3:

Model A

$$C_m(t) = B_o \frac{k_{exo}}{k_{exo} - k_{endo}} (e^{-k_{endo}t} - e^{-k_{exo}t}) \quad (1)$$

C_m denotes measured C_m, B_0 is the initial vesicle pool size, k_{exo} and k_{endo} are rate constants for exo- and endocytosis (Fig. 3, *top trace*).

Model B

$$C_m(t) = B_{0F} k_F t e^{-k_F t} + B_{0S} \frac{k_{exoS}}{k_{exoS} - k_{endoS}} (e^{-k_{endoS}t} - e^{-k_{endoS}t}) \quad (2)$$

C_m denotes measured capacitance. B_{0F} and k_F are the initial vesicle pool size and rate constant of the rapid phase. B_{0S}, k_{exoS}, and k_{endoS} are the initial vesicle pool size and respective rate constants for the slow phase exo- and endocytosis. It was determined experimentally by fitting that the rate constants for rapid exo- and endocytosis are the same within the experimental error.

Model C

$$C_m(t) = B_{0F}(\alpha(k_F t + 1)e^{-k_F t} - e^{-k_F t} - \alpha + 1) + B_{0S} \frac{K_{exoS}}{k_{exoS} - k_{endoS}} (e^{-k_{endoS}t} - e^{-k_{exoS}t}) \quad (3)$$

C_m denotes measured capacitance. B_{0F} and k_F are the initial vesicle pool size and rate constant of the fast phase, respectively. α is the ratio of vesicle membrane area after endocytosis and before exocytosis. B_{0S}, k_{exoS}, and k_{endoS} are the initial vesicle pool size and respective rate constants for slow exo- and endocytosis

The models were tested by fitting the corresponding functions to experimental data and by comparing normalized χ^2 of the fits. In addition, the quality of the fits was examined visually (Fig. 4). Because Models A and B are subsets of Model C, it was not surprising that Model C produced lower χ^2 values than Models A or B. However, only Model C reproduced with high accuracy all measured membrane capacitance records. In contrast, Models A and B completely failed to reproduce excess retrieval (group C) even qualitatively. The only difference between Models B and C is that the latter contains an additional parameter, α, describing the lipid flow through a fusion pore, which is created during exocytosis. We would like to point out that, within the framework of the presented modeling, excess retrieval cannot be reproduced by simply increasing the number of dynamic components unless lipid flow through a fusion pore is taken into account. Although a model with a higher number of dynamic exo–endocytic components would consist of a higher number of free-fitting parameters than Model C, it would certainly fail to reproduce excess retrieval. Thus, we conclude that, within the presented

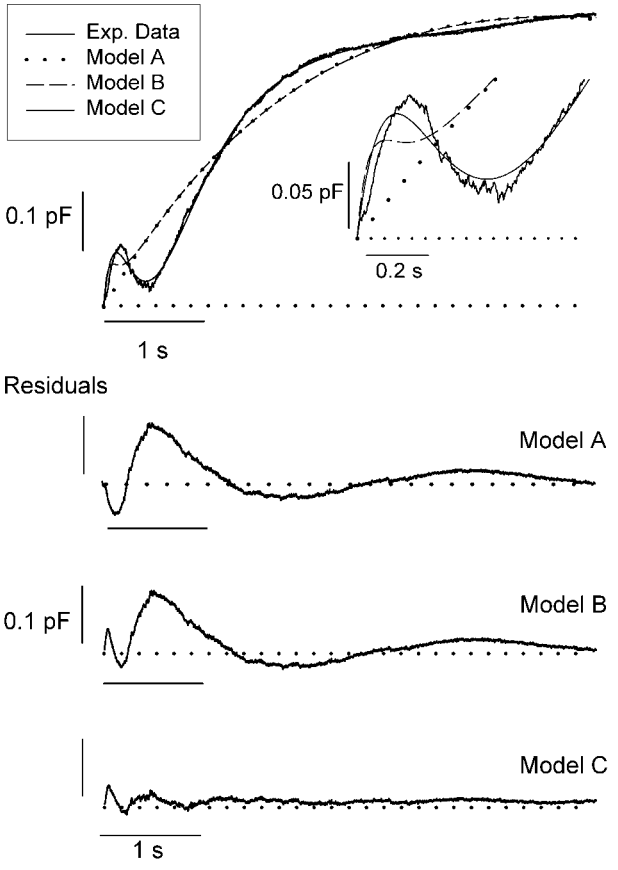

FIGURE 4 Fitting membrane capacitance changes of Type B (*top*) to equations representing Models A, B, and C (see inset for expanded traces). Residuals of fits to respective models are shown below. Note that the best fit was obtained by fitting the equation representing Model C to the data. Parameters of the curves shown on the top panel were as follows: Model C (*dots on line*): $B_{0F} = 0.14$ pF, $B_{0S} = 1.04$ pF, $\alpha = 5.04$, $k_F = 6.49\ s^{-1}$, $k_{exoS} = 1.27\ s^{-1}$, $k_{endoS} = 0$; Model B (*dashed line*): $B_{0F} = 0.13$ pF, $B_{0S} = 0.55$ pF, $\alpha = 1$, $k_F = 16.3\ s^{-1}$, $k_{exoS} = 0.57\ s^{-1}$, $k_{endoS} = 0$; Model A (*thin line*): $B_{0F} = 0$, $B_{0S} = 0.55$ pF, $\alpha = 1$, $k_F = 0$, $k_{exoS} = 0.57\ s^{-1}$, $k_{endoS} = 0$.

scheme, Model C has the minimum number of fitting parameters that can reproduce all the measured flash-induced membrane capacitance responses in rat melanotrophs with high fidelity.

DISCUSSION

The aim of this study was to develop a model describing time-dependent changes in C_m elicited by photolysis of caged calcium (NP-EGTA) in rat melanotrophs. As reported previously (Thomas et al., 1993; 1994; Rupnik et al., 2000), recorded changes in C_m consist of multiple kinetic components. Here, we observed that the time course of C_m during the first 5 s immediately after the UV flash delivery consists of three types of responses, termed type A (monotonic increase in C_m), type B (biphasic increase in C_m), and type C (biphasic increase in C_m with excess retrieval after the first rise in C_m) (Fig. 2). These different categories of responses in C_m appeared to be independent of the peak $[Ca^{2+}]_i$.

Multiphasic C_m responses in neuroendocrine cells have generally been interpreted by a sequential model in which vesicles staged at varying distances from exocytosis undergo progressive fusion (Heinemann et al., 1994; Thomas et al., 1993, Xu et al., 1998). The initial C_m increase is presumed to reflect triggered exocytosis of those vesicles that are fusion competent at the time of the Ca^{2+} increase, whereas later phases of the C_m increase are assumed to reflect the progressive fusion of vesicles that require time-dependent recruitment, docking, or priming steps. However, results showing the selective CAPS-antibody inhibition of the rapid rise in C_m increase (Rupnik et al., 2000) are not easily compatible with a strictly sequential model. Moreover, one cannot neglect the excess retrieval, which appears in approximately 30% of all experiments (Thomas et al., 1994; and Fig. 2) and is also difficult to explain within the framework of a sequential model. Thus, we considered a hypothesis in which rapid and slow exocytosis are mediated by two distinct parallel pathways that use a common pool of vesicles (Fig. 3). Mathematical models of vesicle secretion dynamics based on the above hypothesis were developed and used in quantitative data analysis and interpretation. Model C, which consists of two dynamic components of exo–endocytosis cycle, was shown to reproduce with high fidelity all types of measured responses in rat melanotrophs (Figs. 2 and 4), an observation supporting previously reported existence of biochemically dissimilar mechanisms of exocytosis in melanotrophs (Rupnik et al., 2000) and consistent with a report on chromaffin cells from tissue slices (Voets, 2000). The existence of multiple pathways of exocytosis also appears to be present in other cell types, such as adipocytes (Bogan and Lodish, 1999) and neutrophils (Nusse et al., 1998). In the latter cell type, parallel pathways of exocytosis are associated with distinct calcium sensitivity, which may indicate that vesicles undergoing different exocytic pathways are characterized by particular molecular mechanisms. Indeed, two calcium-sensitive pathways of exocytosis have been associated with different biochemical characteristics (Rupnik et al., 2000). It is likely that different calcium-sensitive mechanisms of glutamate secretion from bipolar neurones (Heidelberger et al., 1994) and from calyx-type synapses (Schneggenburger and Neher, 2000; Bollmann et al., 2000) reflect differences in the molecular organization of exocytic apparatus in these types of neurons.

A possibly important aspect of this work is the attempt to include, in modeling of time-dependent changes in membrane capacitance, a flux of lipids through a reversal closing of the fusion pore (Monck et al., 1990). Inclusion of this process in the model with two dynamic components of exo–endocytosis cycles improves the fitting fidelity in such a way that the model describes well not only distinct types of responses in C_m, but can describe all types of responses

observed in melanotrophs (Figs. 2, 3, and 4). The flux of lipids is driven by the tension gradient between the vesicle membrane and the plasmalemma (Monck et al., 1990; Solsona et al., 1998; Chizmadzhev et al., 1999; 2000). Excess retrieval was exclusively observed to be associated with the rapid exocytosis in rat melanotrophs (Fig. 2; Thomas et al., 1994). This may indicate that the tension gradient between the vesicle and the plasma membrane is different for vesicles in the rapid and slow exocytotic pools. Alternatively, vesicles entering the slow phase of exocytosis may be fusing with the plasma membrane permanently and are retrieved by other endocytic machinery, which then controls the size of the retrieved membrane area, independent of the lipid flow that might have occurred as the fusion pore opened. The mechanism of such a difference in the properties of vesicles in the rapid and slow exocytotic pools is not known. On one hand, different proteins or lipidic structures between interacting membranes may contribute to the two functional populations of vesicles in melanotrophs. Distinct biochemical characteristics of rapid and slow exocytosis (Rupnik et al., 2000; Kreft et al., 1999) support such a mechanism. On the other hand, an interesting question to be elucidated is whether the rapid component of C_m increase reflects exocytosis of vesicles, of which the fusion pore expands more quickly in comparison to vesicles undergoing slow exocytosis. A recent mathematical analysis showed that fusion-pore growth is not affected by tension-driven lipid flux from one membrane to another (Chizmadzhev et al., 2000). It is therefore likely that vesicles undergoing rapid exocytosis are "frozen" in a functional state that favors lipidic flux, hindering the dissipation of tension difference after establishment of the fusion pore. Hence, in such a relatively stable state (i.e., reversible and repetitive fusion-pore opening and closing) the time for lipidic flux to take place would be longer in comparison to the functional state of vesicles undergoing slow exocytosis where the fusion pore may open completely and permanently.

In summary, we have studied C_m elicited by flash photolysis of caged Ca^{2+}. The different types of responses appeared not to be associated with differences in cytoplasmic calcium concentration, an observation consistent with previous reports (Thomas et al., 1993, 1994). To interpret the complex responses, we considered a new mathematical model consisting of two dynamic cycles of exo–endocytosis with a component representing lipid flow during fusion-pore opening after the onset of the rapid rise in C_m. We have demonstrated that the model describes all measured responses with high fidelity. Our results are consistent with the view that complex kinetic changes in C_m are due to distinct pathways of regulated exocytosis. Unlike vesicles entering slow exocytosis, vesicles in rapid exocytosis are characterized by a functional state during which a significant lipid flux can take place.

APPENDIX

For this paper to be self-contained, we hereby derive functions describing capacitance signals as a function of time for different models. The models are based on the vesicle evolution scheme presented in Fig. 3, where vesicles are grouped into three different pools A, B, and C according to their evolutionary state. Pool A contains vesicles that have not reached release-ready state yet and thus cannot directly contribute to the measured signal. The contribution of pool A to the capacitance signals in our models can be neglected. Pool B contains vesicles that can be immediately released upon Ca^{2+} stimulation. Released vesicles enter pool C. Measured capacitance is proportional to the number of vesicles in pool C.

We start our modeling with the simplest case of monophasic slow exocytic response of type A. We assume that the vesicle transition dynamics between different pools is governed by the following set of rate equations:

$$\frac{dN_B}{dt} = -k_{exo}N_B, \tag{A1}$$

$$\frac{dN_C}{dt} = k_{exo}N_B - k_{endo}N_C, \tag{A2}$$

where N_B, and N_C are respective numbers of vesicles in pools B and C. The constants k_{exo} and k_{endo} are rate constants for exo- and endocytosis, respectively. The solution of the above set of equations is given by

$$N_C(t) = \frac{N_{B_0}k_{exo}}{k_{exo} - k_{endo}}(e^{-k_{endo}t} - e^{-k_{exo}t}). \tag{A3}$$

Multiplying Eq. A3 by the capacitance of a single vesicle gives a time dependent capacitance $C_m(t)$ signal, Eq. 1.

A similar set of equations with different coefficients was applied to the rapid phase. However, fitting of the rapid phase data revealed that k_{exo} and k_{endo} for the rapid phase are equal within experimental error. The solution for the rapid-phase capacitance contribution can be found as a limiting value of the Eq. 1 and is given by

$$C_m(t) = B_{0F}k_F te^{-k_F t}, \tag{A4}$$

where B_{0F} and k_F represent initial pool size and rate constant, respectively. Assuming that rapid and slow phase secretory responses evolve in parallel independent pathways, the final solution (Eq. 2) can be readily obtained by summing Eqs. 1 and A4.

Until now, we have not taken into account the possibility that added and retrieved membrane areas per vesicle are not the same. This may occur if the tensions in plasma and vesicle membrane are different, and the fusion pore opens temporarily. In such a case, a significant lipid flow through a fusion pore in a direction of a tension gradient is present. Usually, vesicle-membrane tension is higher than plasma-membrane tension (Monck et al., 1990).

The change in the area of the plasma membrane as a function of time can be written as

$$\begin{aligned}\Delta S(t) &= S_0N_{exo}(t) - S_{endo}N_{endo}(t)\\ &= S_0(N_{exo}(t) - \alpha N_{endo}(t)),\end{aligned} \tag{A5}$$

where $N_{exo}(t)$ is the number of vesicles that were fused and $N_{endo}(t)$, the number of vesicles that were retrieved by time t. S_0 and S_{endo} are the initial

and the final vesicle membrane areas. The parameter α is defined by the ratio

$$\alpha = \frac{S_{endo}}{S_0}. \quad \text{(A6)}$$

$N_{exo}(t)$ and $N_{endo}(t)$ can be calculated from Eqs. A1 and A2. We will do it for the rapid phase, which is associated with excess retrieval. The result is given by

$$N_{exo} = N_{B_0}(1 - e^{-k_F t}), \quad \text{(A7)}$$

$$N_{endo} = N_{B_0}(1 - e^{-k_F t} - k_F t e^{-k_F t}). \quad \text{(A8)}$$

From Eqs. A6, A7, and A8, an expression for the plasma membrane surface as a function of time,

$$\Delta S_F(t) = S_{0F} N_{B_{oF}}(\alpha k_F t e^{-k_F t} + (\alpha - 1)(e^{-k_F t} - 1)) \quad \text{(A9)}$$

is obtained, which is, again, proportional to the measured capacitance. By adding the expression for the slow phase, one obtains the complete solution for the capacitance signal as a function of time (Eq. 3), which is the most general one and contains Eqs. 1, A4, and A6, which describe signals of type A and B as special cases, respectively. Eq. A6 is obtained by setting parameter $\alpha = 1$, corresponding to zero lipid flow through a fusion pore. Similarly, Eq. A4 can be obtained by setting the amplitude of the rapid phase $B_{0F} = 0$.

This work was supported by a Ministry of Sciences and Technology of The Republic of Slovenia (#P3 521 381 and #J3 2344–7421-00) awarded to R.Z. and M.K. We thank S. Grilc for cell cultures.

REFERENCES

Bogan, J. S., and H. F. Lodish. 1999. Two compartments for insulin-stimulated exocytosis in 3T3–L1 adipocytes defined by endogenous ACRP30 and GLUT4. *J. Cell Biol.* 146:609–620.

Bollmann, J. H., B. Sakmann, and J. G. G. Borst. 2000. Calcium sensitivity of glutamate release in a calyx-type terminal. *Science.* 289:953–957.

Carter, T. D. and D. Ogden. 1994. Acetylcholine-stimulated changes of membrane potential and intracellular Ca^{2+} concentration recorded in endothelial cells in situ in the isolated rat aorta. *Pflügers Arch.* 428: 476–484.

Chizmadzhev, Y. A., D. A. Kumenko, P. I. Kuzmin, L. V. Chernomordik, J. Zimmerberg, and F. S. Cohen. 1999. Lipid flow through fusion pores connecting membarnes of different tensions. *Biophys. J.* 76:2951–2965.

Chizmadzhev, Y. A., P. I. Kuzmin, D. A. Kumenko, J. Zimmerberg, and F. S. Cohen. 2000. Dynamics of fusion pores connecting membranes of different tensions. *Biophys. J.* 78:2241–2256.

Heidelberger, R., C. Heinemann, E. Neher, and G. Matthews. 1994. Calcium dependence of the rate of exocytosis in a synaptic terminal. *Nature*. 371:573–575.

Heinemann, C., R. H. Chow, E. Neher, and R. S. Zucker. 1994. Kinetics of the secretory response in bovine chromaffin cells following flash photolysis of caged Ca^{2+}. *Biophys. J.* 67:2546–2557.

Kasai, H. 1999. Comparative biology of Ca^{2+}-dependent exocytosis: implications of kinetic diversity for secretory function. *Trends Neurosci.* 22:88–93.

Kreft, M., S. Gasman, S. Chasserot-Golaz, V. Kuster, M. Rupnik, S. K. Sikdar, F.-M. Bader, and R. Zorec. 1999. The heterotrimeric Gi_3 protein acts in slow but not in fast exocytosis of rat melanotrophs. *J. Cell. Sci.* 112:4143–4150.

Lindau, M., and E. Neher. 1988. Patch-clamp techniques for time-resolved capacitance measurements in single cells. *Pflugers Arch.* 411:137–146.

Mains, R. E., and B. A. Eipper. 1979. Synthesis and secretion of corticotropins, melanotropins and endorphins by rat intermediate pituitary cells. *J. Biol. Chem.* 254:7885–7894.

Monck, J. R., G. Alvarez de Toledo, and J. M. Fernandez. 1990. Tension in secretory granule membranes causes extensive membrane transfer through the exocytotic fusion pore. *Proc. Natl. Acad. Sci. U.S.A.* 87: 7804–7808.

Neher, E., and A. Marty. 1982. Discrete changes of cell membrane capacitance observed under conditions of enhanced secretion in bovine adrenal chromaffin cells. *Proc. Natl. Acad. Sci. U.S.A.* 79:6712–6716.

Neher, E., and R. S. Zucker. 1993. Multiple calcium-dependent processes related to secretion in bovine chromaffin cells. *Neuron.* 10:21–30.

Ninomiya, Y., T. Kishimoto, T. Yamazawa, H. Ikeda, Y. Miyashita, and H. Kasai. 1997. Kinetic diversity in the fusion of exocytic vesicles. *EMBO J.* 16:929–934.

Nusse, O., L. Serrander, D. P. Lew, and K.-H. Krause. 1998. Ca^{2+}-induced exocytosis in individual human neutrophils: high- and low-affinity granule populations and submaximal responses. *EMBO J.* 17:1279–1288.

Rupnik, M., M. Kreft, S. K. Sikdar, S. Grilc, R. Romih, G. Zupančič, T. F. J. Martin, and R. Zorec. 2000. Rapid regulated dense-core vesicle exocytosis requires the CAPS protein. *Proc. Natl. Acad. Sci. U.S.A.* 97:5627–5632.

Rupnik, M., and R. Zorec. 1992. Cytosolic chloride inos stimulate Ca^{2+} induced exocytosis in melanotrophs. *FEBS Lett.* 303:221–223.

Rupnik, M., and R. Zorec. 1995. Intracellular chloride modulates Ca^{2+}-induced exocytosis from rat melanotrophs through GTP-binding proteins. *Pflügers Arch.* 431:76–83.

Schneggenburger, R., and E. Neher. 2000. Intracellular calcium dependence of transmitter release rates at a fast central synapse. *Nature.* 406:889–893.

Solsona, C., B. Innocenti, and J. M. Fernandez. 1998. Regulation of exocytic fusion by cell inflation. *Biophys. J.* 74:1061–1073.

Takahashi. N., T. Kadowaki, Y. Yazaki, Y. Miyashita, and H. Kasai. 1997. Multiple exocytotic pathways in pancreatic β cells. *J. Cell Biol.* 138: 55–64.

Thomas, P., A. K. Lee, J. G. Wong, and W. Almers. 1994. A triggered mechanism retrieves membrane in seconds after Ca(2+)-stimulated exocytosis in single pituitary cells. *J. Cell Biol.* 124:667–675.

Thomas, P., J. G. Wong, A. K. Lee, and W. Almers. 1993. A low affinity Ca^{2+} receptor controls the final steps in peptide secretion from pituitary melanotrophs. *Neuron.* 11:93–104.

Voets, T. 2000. Dissection of three Ca^{2+}-dependent steps leading to secretion in chromaffin cells from mouse adrenal slices. *Neuron.* 28: 537–545.

Walent, J., B. W. Porter, and T. F. J. Martin. 1992. A novel 145 kd brain cytosolic protein reconstitutes Ca^{2+}-regulated secretion in permeable neuroendocrine cells. *Cell.* 70:765–775.

Xu, T., T. Binz, H. Niemann, and E. Neher. 1998. Multiple kinetic components of exocytosis distinguished by neurotoxin sensitivity *Nature Neurosci.* 1:192–200.

Zorec, R., F. Henigman, W. T. Mason, and M. Kordaš. 1991. Electrophysiological study of hormone secretion by single adenohypophyseal cells. *Methods Neurosci.* 4:194–210.

Zupančič, G., L. Kocmur, P. Veranič, S. Grilc, M. Kordaš, and R. Zorec. 1994. The separation of exocytosis in rat melanotroph membrane capacitance records. *J. Physiol. (Lond.).* 480:539–552.